Published OnlineFirst December 2, 2020; DOI: 10.1158/0008-5472.CAN-20-1441

Enhanced Antitumor Immunity via Endocrine Therapy Prevents Mammary Tumor Relapse and Increases Immune Checkpoint Blockade Sensitivity

Gonzalo R. Sequeira[1,2], Ana Sahores[1,3], Tomás Dalotto-Moreno[1], Ramiro M. Perrotta[1], Gabriela Pataccini[1], Silvia I. Vanzulli[4], María L. Polo[1], Derek C. Radisky[5], Carol A. Sartorius[6], Virginia Novaro[1], Caroline A. Lamb[1], Gabriel A. Rabinovich[1,7], Mariana Salatino[1], and Claudia Lanari[1]

ABSTRACT

The role of active antitumor immunity in hormone receptor–positive (HR^+) breast cancer has been historically underlooked. The aim of this study was to determine the contribution of the immune system to antiprogestin-induced tumor growth inhibition using a hormone-dependent breast cancer model. BALB/c-GFP^+ bone marrow (BM) cells were transplanted into immunodeficient NSG mice to generate an immunocompetent NSG/BM-GFP^+ (NSG-R) mouse model. Treatment with the antiprogestin mifepristone (MFP) inhibited growth of 59–2-HI tumors with similar kinetics in both animal models. Interestingly, MFP treatment reshaped the tumor microenvironment, enhancing the production of proinflammatory cytokines and chemokines. Tumors in MFP-treated immunocompetent mice showed increased infiltration of $F4/80^+$ macrophages, natural killer, and CD8 T cells, displaying a central memory phenotype. Mechanistically, MFP induced immunogenic cell death (ICD) *in vivo* and *in vitro*, as depicted by the expression and subcellular localization of the alarmins calreticulin and HMGB-1 and the induction of an ICD gene program. Moreover, MFP-treated tumor cells efficiently activated immature dendritic cells, evidenced by enhanced expression of MHC-II and CD86, and induced a memory T-cell response, attenuating tumor onset and growth after re-challenge. Finally, MFP treatment increased the sensitivity of HR^+ 59–2-HI tumor to PD-L1 blockade, suggesting that antiprogestins may improve immunotherapy response rates. These results contribute to a better understanding of the mechanisms underlying the antitumor effect of hormonal treatment and the rational design of therapeutic combinations based on endocrine and immunomodulatory agents in HR^+ breast cancer.

Significance: Antiprogestin therapy induces immunogenic tumor cell death in PRA-overexpressing tumors, eliciting an adaptive immune memory response that protects mice from future tumor recurrence and increases sensitivity to PD-L1 blockade.

Graphical Abstract: http://cancerres.aacrjournals.org/content/canres/81/5/1375/F1.large.jpg.

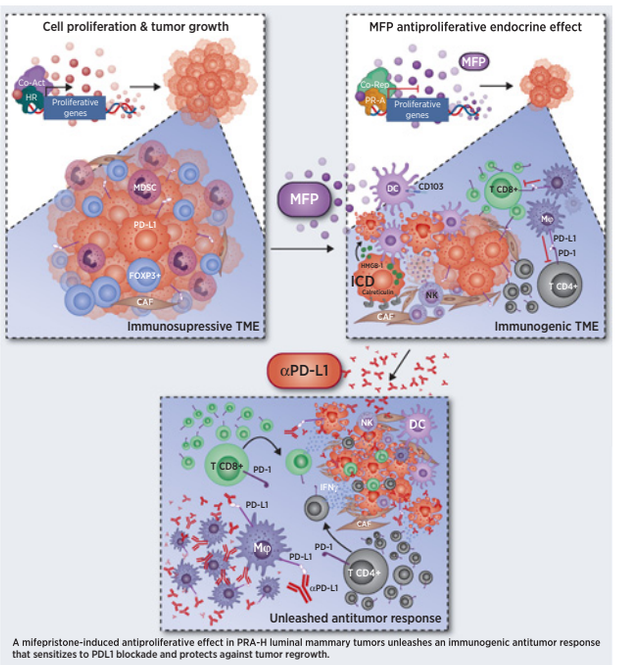

A mifepristone-induced antiproliferative effect in PRA-H luminal mammary tumors unleashes an immunogenic antitumor response that sensitizes to PDL1 blockade and protects against tumor regrowth.

[1]Instituto de Biología y Medicina Experimental (IBYME), CONICET, Buenos Aires, Argentina. [2]Hospital Público de Gestión Descentralizada Dr. Arturo Oñativia, Ciudad de Salta, Salta, Argentina. [3]Instituto de Investigaciones Farmacológicas (ININFA-UBA-CONICET), Facultad de Farmacia y Bioquímica, Universidad de Buenos Aires, Buenos Aires, Argentina. [4]Academia Nacional de Medicina, Buenos Aires, Argentina. [5]Mayo Clinic Comprehensive Cancer Center, Department of Cancer Biology, Jacksonville, Florida. [6]Department of Medicine, University of Colorado, Anschutz Medical Campus, Aurora, Colorado. [7]Facultad de Ciencias Exactas y Naturales, Universidad de Buenos Aires, Buenos Aires, Argentina.

Note: Supplementary data for this article are available at Cancer Research Online (http://cancerres.aacrjournals.org/).

G.R. Sequeira, A. Sahores, and T. Dalotto-Moreno contributed equally as co-first authors of this article.

R.M. Perrotta and G. Pataccini contributed equally as co-authors of the article.

M. Salatino and C. Lanari contributed equally as co-senior authors of this article.

Corresponding Author: Mariana Salatino, Instituto de Biologia y Medicina Experimental CONICET, Vuelta de Obligado 2490, 1428 Buenos Aires, Argentina. Phone: 54-114-783-2869, ext. 1267; Fax: 54-114-786-2564; E-mail: mariansalatino@gmail.com; salatino@dna.uba.ar

Cancer Res 2021;81:1375–87

doi: 10.1158/0008-5472.CAN-20-1441

Published OnlineFirst December 2, 2020; DOI: 10.1158/0008-5472.CAN-20-1441

Introduction

Antitumor therapies based on restoration and activation of immune responses provide a paradigm shift in cancer treatment. These therapeutic strategies involve re-education and re-invigoration of antitumor immune responses. Current immunomodulatory therapies include immune checkpoint blockade (ICB), dendritic cell (DC)-based, and adoptive T-cell transfer (1, 2). Patients treated with ICB have shown durable increased overall survival and progression-free survival responses in a variety of tumors (3–7).

Immunotherapy implementation for breast cancer has been particularly challenging. As mammary carcinomas were traditionally considered immunologically "cold" because of their scant or null T-cell infiltration, therapies based on restoration or activation of immune responses were not a treatment option (8). Tumor mutational burden (TMB) in breast cancer is relatively low and may account for the lack of T-cell infiltration, particularly in hormone receptor–positive (HR^+) tumors (9, 10). However, in breast cancer, high levels of tumor-infiltrating lymphocytes (TIL) were associated with a good prognosis, including reduced recurrence risk (11).

It is already acknowledged that chemotherapy and radiotherapy induce changes in the tumor microenvironment (TME). Radiotherapy increases type I cytokine secretion, upregulates adhesion molecule expression on immune cells, and enhances MHC-I expression on the tumor cell surface, resulting in the recruitment of antigen-presenting cells (APC) and subsequent induction of T-cell activation (12). Chemotherapeutic drugs elicit immunogenic cell death (ICD) characterized by the release of damage-associated molecular patterns (DAMP) such as calreticulin, high mobility box group-1 (HMBG-1), adenosine triphosphate (ATP), and heat shock protein 70 (HSP70) that foster DC maturation, thus priming antitumor immunity (13).

HR^+ breast carcinomas, the most frequent tumors diagnosed in women, have a relatively good prognosis (14). Of these, approximately 70% express estrogen (ER) and progesterone receptors (PR) and are treated with endocrine therapy. We have previously identified a central role for PR isoforms in breast cancer progression and proposed an antiprogestin-based therapy for a subgroup of patients with HR^+ breast cancer (15, 16).

Despite considerable progress, the relevance of antitumor immune response in HR^+ breast tumors is still controversial. Seeking for potential mechanisms that could integrate the endocrine and immune landscapes in HR^+ breast cancer, we investigated whether a short-term antiprogestin therapy with mifepristone (MFP) might influence antitumor immune responses. Here, we show that MFP engages an ICD program capable of unleashing a memory T-cell response, which limits tumor recurrence and increases the sensitivity of HR^+ tumors to ICB. Thus, rational design of therapies targeting both, endocrine and immune compartments, will open new immunotherapeutic opportunities for the treatment of selected patients with breast cancer.

Materials And Methods

Animals

Two-month-old female BALB/c mice from the Animal Facility of *Instituto de Biología y Medicina Experimental* (IBYME) were used. NOD/LySz-scid/IL-2Rgamma null (NSG) and transgenic green fluorescent protein-expressing BALB/c (BALB/c-GFP^+) mice were purchased from The Jackson Laboratory and bred at IBYME. All animals were fed *ad libitum* and kept in air-conditioned room at $20 \pm 2°C$ with a 12-hour light/dark cycle period. All studies were performed according to protocols approved by the IBYME-IACUC committee.

Cell lines

Pancreatic ductal adenocarcinoma human Panc1 cells (ATCC, CRL-1469) and murine CT26 colon cancer cells (ATCC, CRL-2638) were cultured in DMEM or RPMI-1640 supplemented with 10% FBS and 50 μg/mL gentamicin and kept in a humidified 5% CO_2 atmosphere at 37°C. Human T47D-YA and T47D-YB cells were generously provided by Dr. K. Horwitz (University of Colorado). Cells were authenticated by short tandem repeat profiling (Genetica DNA Laboratories Inc.) and cultured as previously described (17). Cell lines were routinely tested for *Mycoplasma* contamination using PlasmoTest (InvivoGen).

Tumors

Mammary carcinomas were originally induced by medroxyprogesterone acetate (MPA) in BALB/c mice. Established tumors express ERα and PR and are maintained by subcutaneous transplantations into syngeneic female mice (18). 59–2-HI and 59-HI are hormone-independent (HI) variants originated from the MPA-dependent 59-HD tumor and, C4-HI and C4–2-HI, from C4-HD. C4-HI and 59–2-HI tumors regress upon antiprogestin treatment and they have higher levels of PR isoform A (PRA) than isoform B (PRA-H tumors), whereas C4–2-HI and 59-HI are MFP-resistant tumors with the opposite PR isoform ratio (18). For *in vitro* studies, 59–2-HI and C4–2-HI were selected because they easily adhere to plastic and grow in primary cultures (18, 19). T47D-YA and T47D-YB xenografts expressing, only PRA or PRB, respectively, were generated as previously described (20, 21). A total of 2×10^5 CT26 or 1×10^6 Panc1 cells were subcutaneously inoculated into BALB/c mice or NSG and NSG-R mice, respectively.

Graft protocol

Femur and tibia bone marrows (BM) from BALB/c-GFP^+ mice were flushed with saline solution. GFP^+ bone marrow cells were centrifuged at $300 \times g$ for 5 minutes, resuspended in red blood cell lysis solution (ACK buffer: 155 mmol/L NH_4Cl; 10 mmol/L $KHCO_3$; 0.1 mmol/L EDTA at pH 7.3), incubated for one minute and washed in PBS. NSG female recipients were injected intravenously with 3×10^7 whole GFP^+ bone marrow cells in 120 μL of PBS. One BALB/c-GFP^+ donor supplied bone marrow for one recipient NSG mouse. To assess bone marrow engraftment, the percentage of circulating GFP^+ cells in NSG-R mice one and two months after bone marrow transplantation, was monitored. Blood (100 μL) was collected in the presence of heparin (Duncan; 5,000 UI/mL) and stained for CD4 and CD8 naïve and memory populations. In addition, cytokine expression after *in vitro* stimulation was determined. Small intestine, skin, liver, spleen and lymph nodes from NSG-R mice were formalin-fixed and paraffin-embedded (FFPE) for histologic evaluation (hematoxylin and eosin) or stained for GFP expression by IHC (21).

In vivo experiments

59–2-HI epithelial tumor cells (1.5×10^5, 100 μL in PBS) were subcutaneously injected into BALB/c, NSG or NSG-R mice. Tumor size was monitored every three days using a *Vernier* caliper and tumor area was measured as $L \times W$. When tumors reached 25 mm^2, animals were treated with MFP (Sigma). High MFP doses (6-mg pellets or 10 mg/kg/d) were used to induce complete tumor regression and lower doses (0.1 mg pellets or 0.4 mg/kg/d) in combined treatments with anti–PD-L1 and to ensure remaining tumor tissue (21). In combined treatments, four days after MFP-treatment initiation, PD-L1–blocking antibody (10 mg/kg intraperitoneal every two days; InVivoMAb; BioXcell) or isotype control were administered.

Published OnlineFirst December 2, 2020; DOI: 10.1158/0008-5472.CAN-20-1441

Excised tumors were divided into three fragments that were: Fixed in 10% formalin, mechanically and enzymatically minced for FACS analysis (22), and kept in 4% cold paraformaldehyde overnight and transferred to 20% sucrose for 24 hours to preserve GFP fluorescence (21). Frozen sections were processed as described previously (21) and nuclei counterstained with propidium iodide (PI; Sigma). Fluorescence was analyzed by confocal microscopy (Nikon Eclipse E800).

For re-challenge experiments, mice were anesthetized with ketamine (100 mg/kg) and xylazine (10 mg/kg) and tumors were excised. Three weeks later, mice were re-inoculated with 59–2-HI tumor cells (1.5×10^5) in the contralateral flank (19).

Flow cytometry (FACS)

Tumor-derived cells and peripheral blood mononuclear cells (PBMC) were stained for expression of cell surface markers, and cytokine production was assessed as described in Supplementary Materials and Methods.

Microarray analysis

We used C4-HD tumors growing in MPA-treated BALB/c mice. When tumors reached 50 mm^2, MPA pellets were removed by surgery and MFP (10 mg/kg/d) was inoculated subcutaneously. Two days later, tumors were excised and fixed in formalin. RNA was extracted from FFPE tumors using the RNeasy FFPE kit (Qiagen; #73504). RNA integrity was assessed with an Agilent Bioanalyzer 2100 (Agilent Technologies) prior to labeling and hybridization to Gene Chip Mouse Genome 430 2.0 (Affymetrix, #900497) according to the manufacturer's instructions. Data are available in the Gene Expression Omnibus database (GSE161012). The detailed bioinformatic analyses, with differentially expressed genes (DEG), are described in Supplementary Materials and Methods.

IHC

IHC was performed as described preciously (23). Primary antibodies were calreticulin (sc-373863) and HMGB-1 (sc-56698; Santa Cruz Biotechnology) and GFP (Cell Signaling Technology; 2956). A pathologist (S.I. Vanzulli) performed a blind semi-quantitative scoring and the staining was graded as negative (0), weak (1), moderate (2), and strong (3). The staining score (scale, 0–300) results from the product between positivity (0%–100%) and intensity.

Tumor and DC cocultures

Immature mouse DC, bone marrow cells were incubated for 8 days in 10% FBS-supplemented RPMI with recombinant mouse GM-CSF (20 ng/mL; Peprotech; ref. 24). Immature $CD11c^+$ cells were then isolated with microbeads (Miltenyi). 59–2-HI and C4–2-HI cell suspensions were cultured (19) for two days and cells were treated with MFP or etoposide (20 μmol/L) for 24 or 48 hours. Tumor and immature DC were cocultured (1:1) for 24 hours. DC activation was assessed as the percentage of MHC-II^+ and $CD86^+$ cells within the live (Zombie $Aqua^{neg}$) $CD45^+CD11c^+$ population.

Statistical analysis

GraphPad Prism 6.0 software was used. The Shapiro Wilk test was used to evaluate normal distribution. Comparisons between two groups were analyzed by Mann–Whitney-Wilcoxon tests or student *t* tests depending on their normal distribution. ANOVA or Kruskal Wallis were used for multiple comparisons, followed by Tukey tests to compare selected groups. Tumor growth curves were analyzed by two-way ANOVA with repeated measures. In re-challenge assays, contingency table analysis followed by the Fisher's exact test was used. The log-rank test was used to analyze Kaplan–Meier curves.

Results

Development of an immunocompetent chimeric mouse model

To study the immune response upon antiprogestin therapy, we developed immunocompetent NSG-R mice by reconstituting NSG mice with bone marrow from BALB/c-GFP mice. Engraftment success was evaluated by quantification of GFP^+ cells in the bone marrow (**Fig. 1A**; Supplementary Fig. S1A) and blood (**Fig. 1B**) of NSG-R mice. Circulating CD4 effector T cells ($CD44^+CD62L^{neg}$) and CD8 central memory ($CD44^+CD62L^{hi}$) T cells in NSG-R mice were comparable to BALB/c or donor BALB/c-GFP^+ mice (**Fig. 1C**). In addition, CD8 and CD4 T cells from peripheral blood of NSG-R mice were functional, as they elicited cytokine production, including IFN-γ, TNF, and IL-2 upon PMA/Ionomycin stimulation (**Fig. 1D**), although slight differences in cytokine production of CD8 T cells between NSG-R and BALB/c-GFP^+ mice were observed. We also identified GFP^+ lymphocyte clusters in bone marrow, lymph nodes, structures resembling Peyer patches in the small intestine sub-mucosa and spleen in NSG-R mice with cell densities comparable with those of BALB/c mice (Supplementary Fig. S1A–S1D). No histological differences were observed between the small intestine, skin, and liver from NSG-R compared with control mice (Supplementary Fig. S1E). Moreover, CD4 and CD8 T-cell frequencies were similar (**Fig. 1C**), ruling out a possible graft versus host (GvH) reaction. We also found that immune reconstitution led to a recovery of the spleen/animal weight ratio (**Fig. 1E**) in NSG-R mice. These mice proved to be immunocompetent because they rejected the growth of a xenogeneic pancreatic human tumor cell line (**Fig. 1F**) confirming that NSG-R mice have a restored and functional immune compartment.

Antitumor effects of MFP are similar in immunodeficient and immunocompetent hosts

To investigate the participation of the immune system in antiprogestin-mediated tumor regression, we used 59–2-HI tumors (18). This is an optimal model to evaluate the effects of endocrine therapies because tumors express higher levels of isoform A than B, referred to as PRA-H, and consequently regress upon MFP treatment (23).

We inoculated 59–2-HI tumors into NSG-R or NSG mice that were treated with low MFP doses to avoid complete regression. Antiprogestin treatment impaired tumor growth (**Fig. 2A**) in both animal models and induced immune infiltration of GFP^+ cells in NSG-R (**Fig. 2B**; Supplementary Fig. S2A and S2B). Thus, our results suggest that NSG-R mice are suitable to study changes in the TME after antiprogestin treatment.

MFP alters the immune profile of tumor infiltrates and augments antitumor immunity

We have shown in HR^+ tumors that short-term antiprogestin treatment induced tissue remodeling, vascular normalization, and macrophage and T-cell infiltration (25). To dissect the impact of MFP treatment on tumor immune landscape, we evaluated the immune infiltrates of NSG-R mice bearing 59–2-HI tumors. We found that MFP-treated NSG-R mice displayed an increased infiltration of $F4/80^+$ macrophages (**Fig. 2C**, left). Regarding the lymphocytic population, we observed an increase in $CD3^{neg}CD49^+$ natural killer (NK) cells (**Fig. 2C**, right) and cytotoxic $CD8^+$ T cells (**Fig. 2D**) infiltration and a decrease in the frequency of $Foxp3^+$ regulatory T (Treg) cells, leading to a lower Treg/CD8 ratio (**Fig. 2E**) in MFP-treated mice.

Published OnlineFirst December 2, 2020; DOI: 10.1158/0008-5472.CAN-20-1441

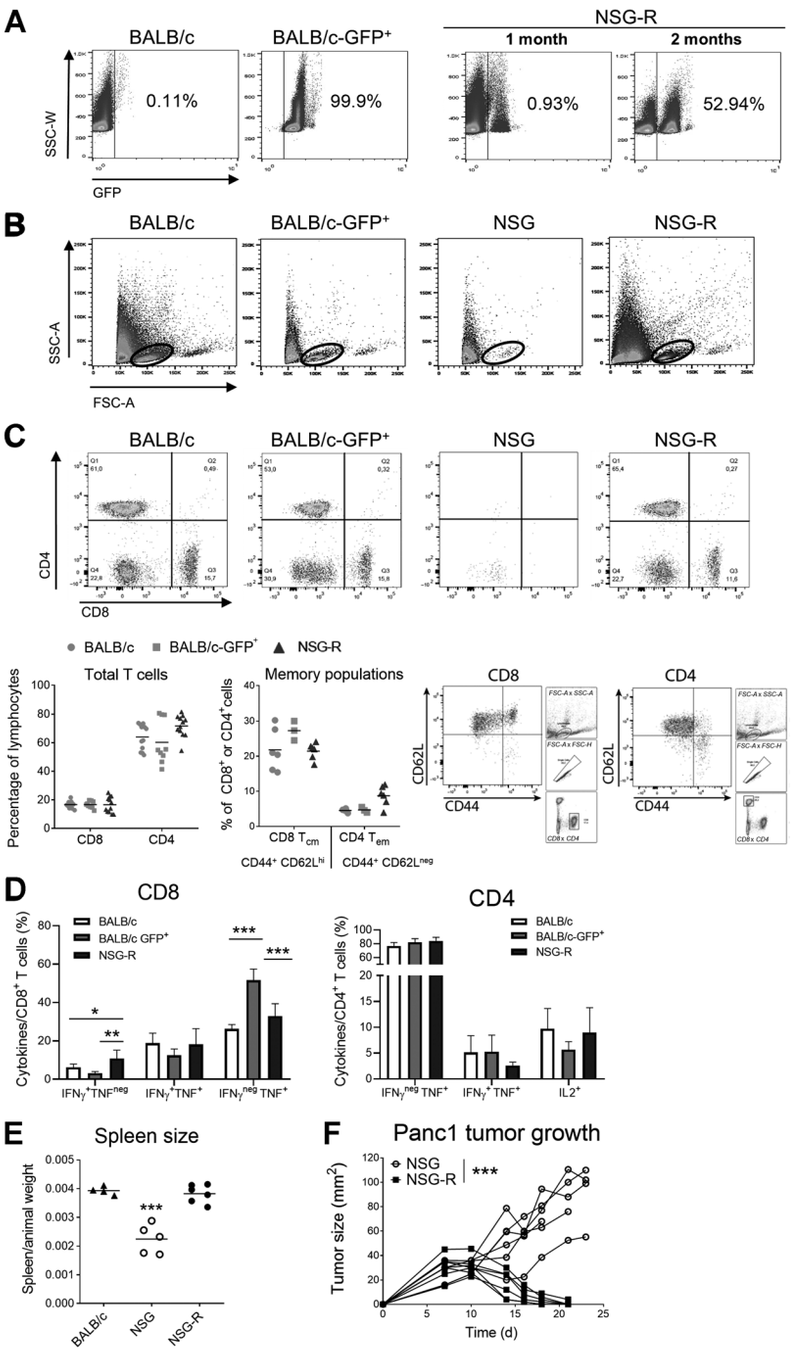

Figure 1.

Generation of immunocompetent NSG-R mice. Bone marrow cells from immunocompetent BALB/c-GFP$^+$ mice were injected intravenously into female recipient immunodeficient mice (NSG) to generate an NSG-BM-GFP$^+$ (NSG-R). BALB/c, BALB/c-GFP$^+$, NSG and NSG-R mice were compared. **A,** The percentage of GFP$^+$ circulating cells was determined by FACS analysis ($n = 4$). **B** and **C,** Lymphoid population (circle) was analyzed by FSC versus SSC (**B**). Total CD8$^+$ and CD4$^+$ T cells frequencies, CD8 central memory T cells (CD8 T_{cm}), CD4 effector memory T cells (CD4 T_{em}), and representative dot plots of CD8 T_{cm} and CD4 T_{em} with their gating strategies are shown (**C**). **D,** PBMCs ($n = 3$) were stimulated with PMA/Ionomycin and monensin for 3 hours and cytokine expression was analyzed (right; mean ± SEM) by FACS. **E,** Spleens were weighed and the ratio between spleen and animal weight was calculated ($n = 5$/group). **F,** NSG-R and NSG mice were challenged with 1×10^7 xenogeneic Panc1 tumor cells in the inguinal flank and tumor size was monitored ($n = 5$/group). The mean ± SD of a representative experiment of other two is shown. *, $P < 0.05$; **, $P < 0.01$; ***, $P < 0.001$.

Moreover, CD8 and CD4 T cells were enriched in central (CD44$^+$CD62L^{hi}) and effector (CD44$^+$CD62L^{neg}) memory populations (**Fig. 2F**). Similar results were found in BALB/c mice (**Fig. 2G–L**) where MFP also induced tumor growth inhibition (**Fig. 2G**). CD45$^+$ cell infiltration (**Fig. 2H**) was enhanced upon MFP treatment, and importantly, we also observed an enrichment in NK cell and in CD4$^+$ and in CD8$^+$ T-cell populations along with a reduction in Foxp3$^+$ Tregs cells (**Fig. 2I**). In contrast, we observed an overall reduction in the infiltration of immunosuppressive MDSCs, CD11b$^+$Ly6G$^+$Ly6C^{neg}, and CD11b$^+$Ly6G^{neg}Ly6C$^+$ (Supplementary Fig. S3A). On this note, MFP systemically affected splenic granulocyte MDSC population (Supplementary Fig. S3B). Although F4/80$^+$ macrophages frequency was unaltered, they displayed an elevated MHC-II and CD206 expression (**Fig. 2J**), reflecting an M2-activated phenotype. Among other myeloid populations in the TME, MFP treatment promoted an increased frequency of CD103$^+$ cross-presenting DC (**Fig. 2K**). No significant changes in CD8$^+$ nor CD4$^+$ T effector memory populations were observed (although a trend was evident). Interestingly, CD4$^+$ T cells upregulated PD-1 expression (**Fig. 2L**), suggesting a dysfunctional phenotype. Notably, *in vivo* exposure to MFP did not upregulate PD-L1 expression in 59–2-HI tumor cells (Supplementary Fig. S4A), but instead, upregulated PD-L1

Published OnlineFirst December 2, 2020; DOI: 10.1158/0008-5472.CAN-20-1441

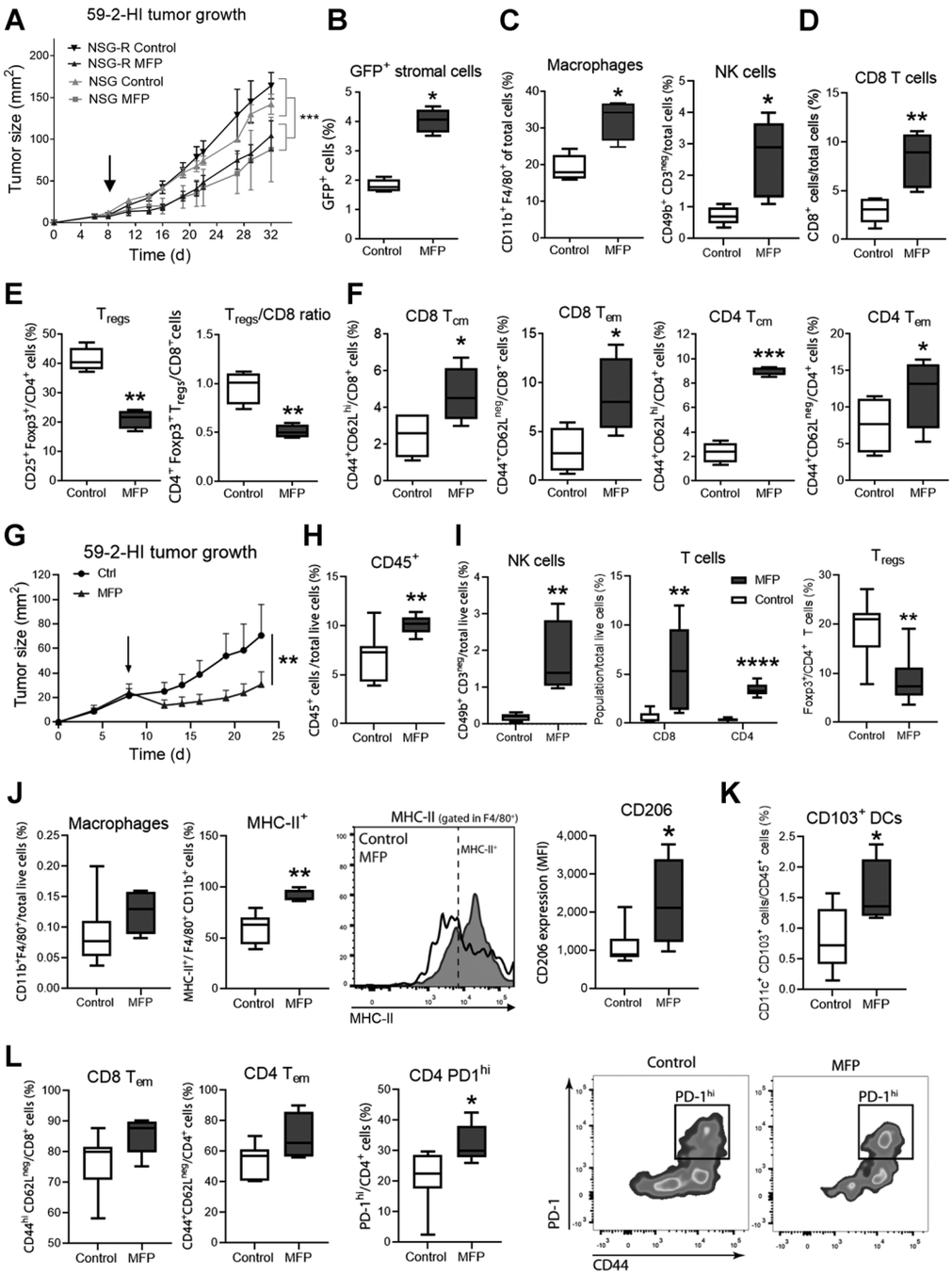

Figure 2.

MFP treatment alters the immune composition of the TME of 59–2-HI tumors growing in NSG-R (**A–F**) or BALB/c mice (**G–L**). **A** and **G,** 59–2-HI tumors were transplanted into NSG or into NSG-R (**A**) or into BALB/c (**G**) mice and treated or not with low MFP doses (0.4 mg/kg/d; $n = 6$/group). Tumor growth was measured. Arrow, treatment initiation. **B–F,** Tumors were minced and analyzed by FACS. **B,** Quantification of GFP^+ cells. **C–F**, Frequency of $CD11b^+F4/80^+$ macrophages and $CD3^{neg}CD49^+$ NK cells is shown (**C**). The percentage of $CD8^+$ cytotoxic cells (**D**), of $CD4^+CD25^+Foxp3^+$ Treg cells, and the Tregs/CD8 ratio is depicted (**E**). Frequency of CD8 and CD4 T-cell, both $CD44^+CD62L^{hi}$ (central memory) and $CD44^+CD62L^{neg}$ (effector memory) was described previously (**F**). **G–L,** Tumors from BALB/c mice treated with MFP (0.4 mg/kg/d; $n = 6$–8/group) were minced and analyzed by FACS. The frequency of $CD45^+$ (**H**), NK, $CD4^+$, $CD8^+$, and $Foxp3^+$ Tregs cell populations (**I**) is shown. The macrophage infiltration and activation status (**J**), and the frequency of $CD103^+$ DCs (**K**) is shown. Frequency of CD8 Tem and CD4 Tem populations and PD-1 expression in $CD4^+$ T cells is shown (**L**). The mean ± SD from a representative experiment of three for NSG-R and two for BALB/c mice is shown. *, $P < 0.05$; **, $P < 0.01$; ***, $P < 0.001$; ****, $P < 0.0001$.

Published OnlineFirst December 2, 2020; DOI: 10.1158/0008-5472.CAN-20-1441

expression in $CD45^{neg}$ cells and in $F4/80^{+}$ macrophages within the tumor (Supplementary Fig. S4B and S4C), supporting an M2 phenotype of these cells.

We next explored whether MFP could prime and/or expand tumor-specific T-cell clones. Importantly, when lymphocytes isolated from tumor-draining lymph nodes (TDLN) from MFP-treated mice were activated *ex vivo* with tumor antigen-pulsed DCs, an increased proportion of CD4 T cells produced IFN-γ (Supplementary Fig. S5A). No differences were observed in the frequency of IFN-γ–producing CD8 T cells, but MFP increased the frequency of activated $CD69^{+}$ $CD8^{+}$ and $CD4^{+}$ T cells (Supplementary Fig. S5A). These results are consistent with an augmented T-cell priming and/or a de-repressed T-cell expansion upon MFP treatment. In that line, even when we did not detect differences in the frequency of Tregs in the TDLN, there was a significant reduction in CTLA-4 expression in MFP-treated mice, suggesting a lower suppressive phenotype (Supplementary Fig. S5B). Altogether, our data show that MFP treatment induces a strong remodeling of the immune TME that may tilt the balance to an antitumor immune response. However, these changes in the TME do not appear to collectively inhibit tumor growth any further in NSG-R mice (**Fig. 2A**) that may suggest that T-cell dysfunction (via PD-L1/PD-1 pathway) or other inhibitory programs may be occurring.

We next sought for the underlying mechanisms that correlated with the immune remodeling elicited by MFP. After gene expression profiling, an unsupervised clustering revealed two main gene groups (**Fig. 3A**). Gene set enrichment analysis of downregulated processes revealed an enrichment in cell-cycle and mitotic-related pathways, which is consistent with the antiproliferative effect of MFP (**Fig. 3B**; Supplementary Table S2). Interestingly, we also observed a significant enrichment in several immune related gene ontology (GO) terms in MFP-treated tumors (**Fig. 3C**; Supplementary Table S1). Using a 32-gene ICD set (26), we observed a significant enrichment of this process in MFP-treated tumors (**Fig. 3D** and **E**) that could be positively associated with a more effective immune cell priming. Next, we studied the DEGs induced by MFP during early regression identifying 1,105 upregulated and 1,039 downregulated transcripts (**Fig. 3F**; Supplementary Table S3). DEGs were studied for overrepresentation of different GO terms revealing an upregulation in the inflammatory response process (**Fig. 3G**; Supplementary Table S4) with an enrichment in proinflammatory chemokines, cytokines, and immune-related receptors (**Fig. 3H**; Supplementary Table S5). Thus, in addition to its well-recognized effects on the proliferation/apoptosis of PRA-H tumors, MFP also triggers a significant remodeling of the immune profile of the TME fostering the activation of pro-inflammatory transcriptional programs.

MFP triggers ICD mediated by DAMPs in hormone-sensitive cells

Next, we explored whether the mechanism by which MFP treatment primed antitumor immunity involved an ICD. We evaluated whether MFP induced changes in the expression or subcellular localization of DAMPs, as calreticulin and HMGB-1, by IHC staining in the MFP-sensitive tumors and in the resistant variants (18). We also assessed DAMPs expression in the MFP-sensitive T47D-YA human xenograft and its resistant counterpart, T47D-YB (23). We found that MFP increased cytosolic compartmentalization of calreticulin in sensitive murine tumors and in human-sensitive xenografts (**Fig. 4A**), whereas no significant changes were detected in the MFP-resistant variants (**Fig. 4A**, bar graph). Similarly, although HMGB-1 expression showed a nuclear localization in the human sensitive T47D-YA xenografts, we observed a clear shuttling from the nuclei toward the cytoplasm upon MFP treatment (**Fig. 4B**).

To determine whether changes in DAMPs expression may influence DC function, we evaluated the ability of MFP-treated sensitive cells to regulate DC maturation in coculture experiments. In agreement with DAMPs exposure, MFP-treated cells upregulated MHC-II and CD86 expression on bone marrow–derived DCs (BMDC; **Fig. 4C**). Conversely, exposure to MFP-resistant tumor cells did not produce changes associated to DC maturation, suggesting that MFP induces ICD, only on MFP-sensitive tumors. Etoposide, a topoisomerase inhibitor (27), was used as an ICD-positive control. Upon etoposide exposition, MFP-resistant cells induced higher MHC-II and CD86 expression on DC after coculture (**Fig. 4C**). The differential response to etoposide of MFP-sensitive and -resistant tumor cells may be due to differences in their proliferation rates because MFP-resistant cells have a higher proliferation index (21). These results emphasize the ability of MFP to trigger ICD in selected HR^{+} tumor cells.

MFP treatment triggers an immunological memory that protects mice from a subsequent tumor challenge

The alterations observed in the tumor immune composition between MFP-treated NSG and NSG-R mice, along with the enrichment on an inflammatory and immune response gene signature, prompted us to hypothesize that MFP could promote a protective immunological memory. Thus, we re-challenged MFP-treated mice with the same tumor. NSG-R mice bearing 59–2-HI tumors were treated with MFP and then tumors and pellets were removed. Three weeks later, mice were re-inoculated with the same tumor into the contralateral flank and tumor growth was monitored until controls reached an ethical maximal size (the complete list of treatments and group distribution are shown in **Fig. 5A**). Tumors grew in 100% of NSG and NSG-R mice control groups. Surprisingly, only 45% of NSG-R mice that had been previously treated with MFP developed tumors after re-challenge (**Fig. 5A** and **B**). Importantly, MFP treatment before re-challenge significantly improved overall survival in NSG-R mice (**Fig. 5C**). On the contrary, untreated controls in both NSG-R and NSG groups reached the maximal ethical size, suggesting a lack of antitumor protection (**Fig. 5C**).

We further validated these findings using BALB/c mice (**Fig. 6A**). MFP treatment also induced a protective memory response in these re-challenge experiments (**Fig. 6B** and **C**). The specificity of the antitumor memory immune response was confirmed by re-challenging mice with syngeneic CT26 colorectal tumor that grew with similar kinetics in all animals (**Fig. 6D**).

MFP treatment increases ICB response in HR^{+} tumors

Several preclinical studies have indicated a synergism between chemotherapy and ICB by anti–PD-1/PD-L1 agents (12). On the basis of the evidence that MFP induced both ICD and T-cell infiltration, we evaluated whether priming of an antitumor immune response by MFP could render PRA-H tumors sensitive to ICB. To this end, mice bearing 59–2-HI tumors were treated with MFP and anti–PD-L1, alone or in combination. We used an anti–PD-L1 antibody, because it was the first immune-checkpoint inhibitor approved for breast cancer and because high expression of PD-L1 was detected in the TME (Supplementary Fig. S4). MFP impaired tumor growth, whereas PD-L1 blockade alone partially inhibited tumor growth (**Fig. 7A**). However, when combined with MFP, anti–PD-L1 treatment promoted a pronounced tumor regression (**Fig. 7A**), inducing an antitumor immune profile (**Fig. 7B–F**). Particularly, in the combinatorial regimen we found an increased CD8/Tregs ratio within the TME (**Fig. 7B**) that results from a decrease in $Foxp3^{+}$ Tregs and an increase in $CD8^{+}$ T-cell populations frequencies (**Fig. 7B**). Importantly, we observed an induction of systemic

Published OnlineFirst December 2, 2020; DOI: 10.1158/0008-5472.CAN-20-1441

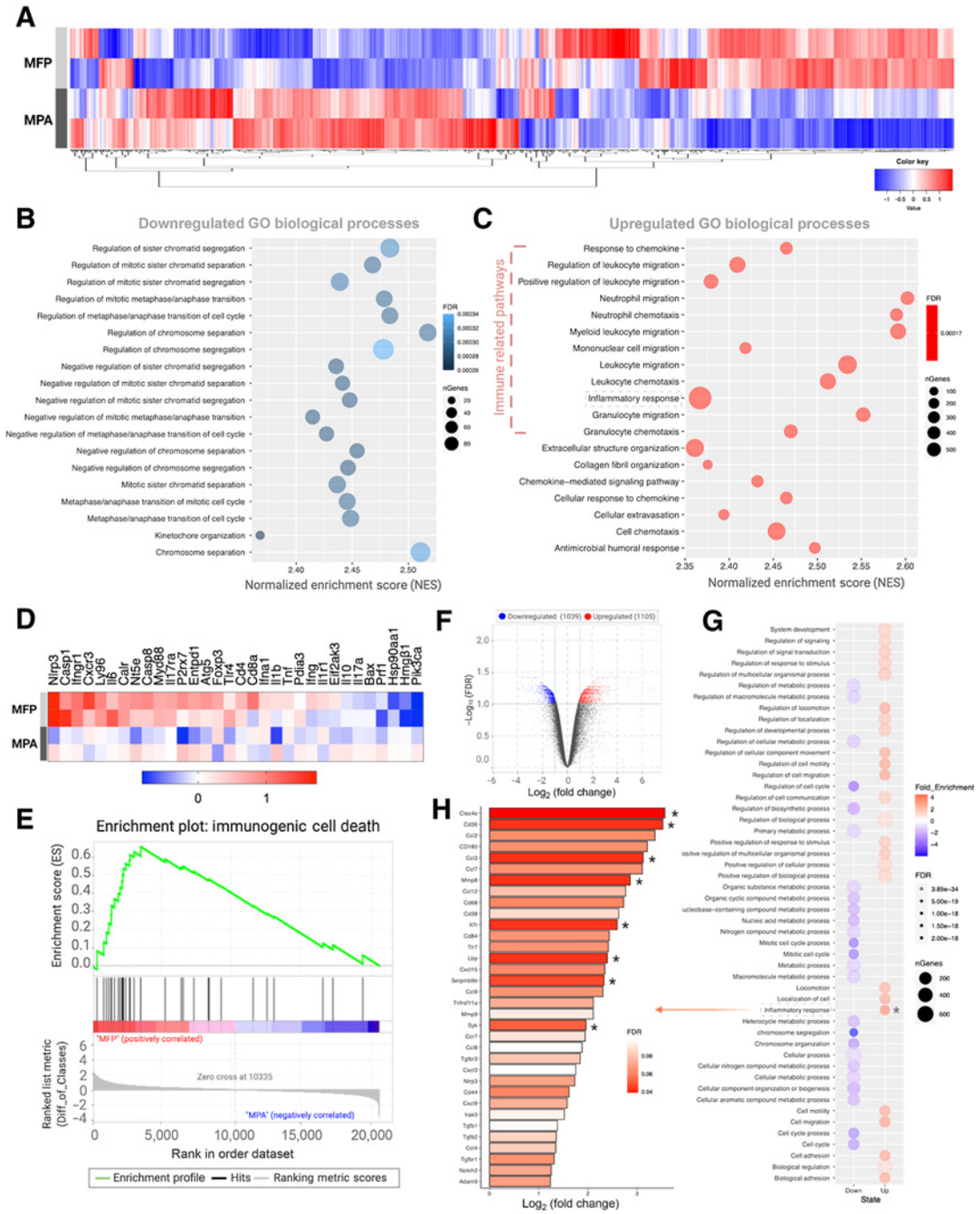

Figure 3.

MFP treatment activates a transcriptional program involved in inflammatory and immune response. **A,** Unsupervised hierarchical clustering of standardized expression values (Z-score) for the top 10,000 most variable genes. **B** and **C,** Top 20 statistically significant (FDR < 0.01) downregulated (**B**) or upregulated (**C**) GO biological processes in MFP-treated mice after gene set enrichment analysis (pre-ranked GSEA). *x*-axis indicates the absolute value of the enrichment score normalized across analyzed gene sets (NES). **D** and **E,** ICD gene set (**D**), Z-score values, and enrichment plot after GSEA analysis (FDR < 0.01; **E**). **F** and **G,** All differential expressed genes (FDR < 0.1 and FC>2; DEGs; **F**). Top 20 up/downregulated pathways (FDR < 0.01; **G**). *, Inflammatory response GO was also upregulated using DEG (FDR < 0.05 and FC > 2). **H,** List of the 24 genes upregulated in the inflammatory response GO. The *x*-axis is expressed in Log_2(FC; FC > 2) and color scale FDR values. Color scale indicates fold enrichment, bubble opacity denotes the FDR value, and the bubble size represents the number of genes in the gene set after filtering out those genes not present in the expression dataset.

Published OnlineFirst December 2, 2020; DOI: 10.1158/0008-5472.CAN-20-1441

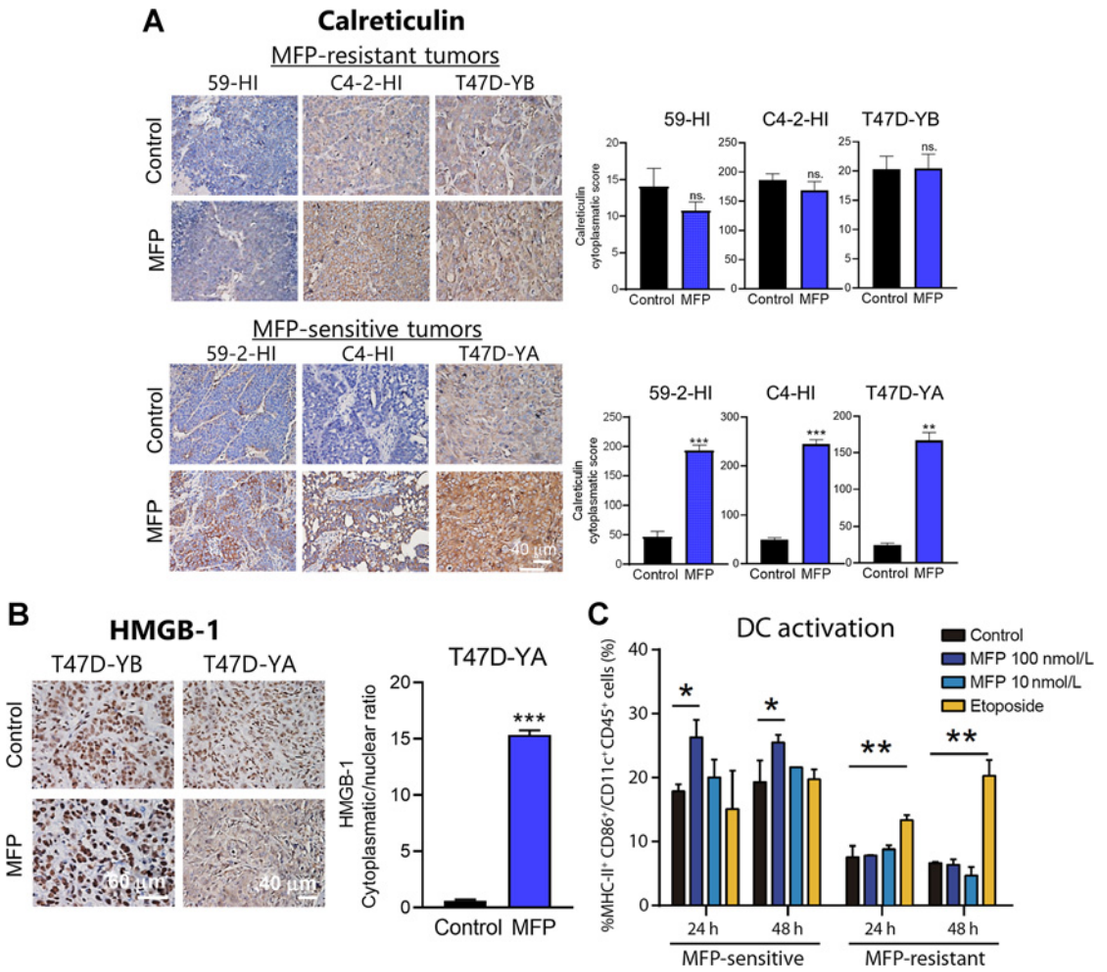

Figure 4.

MFP treatment increases DAMPs exposure and activates DCs only in hormone-sensitive tumors. **A** and **B,** Calreticulin (**A**) and HMGB-1 (**B**) expression was evaluated by IHC in MFP-sensitive and -resistant tumors after six days of MFP-treatment (10 mg/kg/d; $n = 4$/group). Graphs represent quantification of calreticulin cytoplasmic score (**A**). Quantification of cytoplasmic and nuclear HMGB-1 scores was used to calculate their ratio in MFP-treated or control T47D-YA xenografts (**B**). **C,** Syngeneic bone marrow–derived immature DCs were cocultured for 24 hours with MFP-sensitive or MFP-resistant tumor cells that had been previously treated or not with MFP or with etoposide (20 µmol/L) for 24 or 48 hours. The frequency of activated MHC-II$^+$CD86$^+$/CD45$^+$CD11c$^+$ DCs was determined by FACS. The mean ± SEM of three experiments is shown; *, $P < 0.05$; **, $P < 0.01$; ***, $P < 0.001$; ns, nonsignificant.

central and effector memory CD8 T-cell populations (**Fig. 7C**), but not in memory CD4 T cells (**Fig. 7D**). The combination also promoted an increase in the proportion of CD8 and CD4 T cells producing IFN-γ and TNF (**Fig. 7E** and **F**). Interestingly, we found that the effect of each individual treatment merges when MFP and anti–PD-L1 were applied together (**Fig. 7B**–**F**). Decreased frequency of Treg in TME was a feature of MFP (**Fig. 7B**), whereas expansion of polyfunctional memory CD8 T-cell population was linked to PD-L1 blockade (**Fig. 7C**–**F**). Thus, in selected HR$^+$ tumors, MFP induces radical remodeling of the TME through activation of proinflammatory and ICD transcriptional programs, which prime an adaptive memory T-cell response that is ultimately potentiated by PD-L1 blockade.

Discussion

Breast cancer is the most commonly diagnosed cancer in women around the world (28). Although current treatments are often initially successful with patients with HR$^+$ breast cancer, there is still significant incidence of relapse and subsequent mortality. Despite the initial excitement after the approval of the anti–PD-L1 antibody in combination with chemotherapy for patients with metastatic TNBC (29), its effectiveness has recently been questioned (Phase 3, IMpassion131 trial) and new immunotherapy combinatorial regimens are still necessary. HR$^+$ breast cancer has been traditionally considered as non-immunogenic and, thus, the opportunities for immune intervention have been postponed (30). In this work, we show that MFP-treated PRA-H luminal mammary carcinomas promote tumor ICD, which in turn elicits a memory T-cell response protecting the host from future recurrences and sensitizing HR$^+$ tumors to PD-L1 blockade. Although MFP has an endocrine-related inhibitory effect on tumor growth that is independent of the immune system, the remodeling of the immune composition of the TME that occurs during the tumor inhibition can be exploited therapeutically.

Published OnlineFirst December 2, 2020; DOI: 10.1158/0008-5472.CAN-20-1441

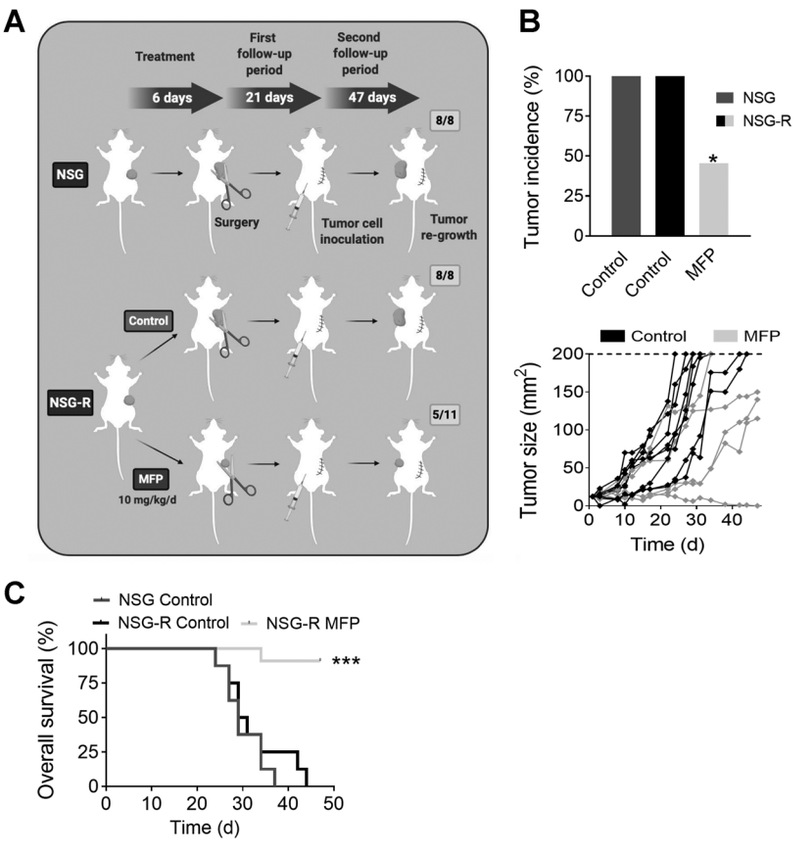

Figure 5.

MFP treatment induces an immune-protective memory in NSG-R mice. **A,** Schematic diagram of the experimental design. 59–2-HI cells were injected into the flank of NSG-R mice. When tumors reached 20–30 mm^2, animals were subcutaneously treated with high MFP doses (10 mg/kg/d) or remained untreated. After six days, tumors were surgically excised. After three weeks, mice were re-challenged with a second injection of 59–2-HI cells into the contralateral flank. Secondary tumor growth was monitored. Created with BioRender.com. **B,** Tumor incidence indicates the percentage of animals in which a tumor was detected. Curves represent individual tumor growth kinetics. **C,** Animals were euthanized when tumors reached 200 mm^2. Overall survival of re-challenged mice is depicted in a Kaplan–Meier curve (n = 8–11/group); *, $P < 0.05$; ***, $P < 0.001$.

The generation of the NSG-R chimeric mice (NSG + BM of BALB/c-GFP$^+$) allowed us to evaluate the contribution of the immune system to MFP-driven tumor growth inhibition. NSG mice are severely immunodeficient as a consequence of the complete disruption of the β2m and γc chains (31, 32). The advantage of the NSG-R model is that engrafted cells are easily detected in the host by means of GFP staining but they also preserve residual NSG-BM activity, related to the mesenchymal contributions of endothelial cells, fibroblasts, pericytes, and macrophages (33, 34). Consequently, 59–2-HI tumors growing in NSG-R mice are infiltrated by a combination of donor transplanted and recipient BMDC. However, only BMDC from BALB/c-GFP$^+$ donors (Supplementary Fig. S1; **Fig. 5**) are functional and capable of evoking an effective antitumor immune response. Remarkably, NSG-R and BALB/c mouse models were optimal for functional analysis, both respond equally to MFP treatment and share many similarities in tumor immune composition and antitumor memory response, even though the correspondence between the two models was not absolute. As described, we did observe some differences in T-cell cytokine production (**Fig. 1D**). In the same line, NSG-R mice were less efficient to reject 59–2-HI tumors after the re-challenge (**Figs. 5** and **6**) that may reveal that chimeric mice could still have some inherent immunodeficiency compared with BALB/c mice. Notably, NSG-R mice were healthy and displayed no evidence of physical or behavioral abnormalities related to the BM-GFP$^+$ engraftment. Moreover, no signs of GvH reaction were observed in NSG-R mice. This might occur because NOD and BALB/c mice share two haplotypes. A similar finding was reported previously describing a GvH only in old animals (35). The technique presented herein offers a highly reproducible and low-cost method to evaluate the bone marrow contribution to pathophysiological processes and is especially suited to carry out immune recovery strategies.

Tamoxifen and aromatase inhibitors have been the standard of care in patients with HR$^+$ breast cancer. Nevertheless, some of these tumors fail to respond to treatments and many patients relapse. In the past years, attention has been shifted toward the tumor-promoting role of PR (36) and our group has dissected the role of PR isoforms, PRA and PRB, in breast cancer progression (15, 23). We found that a high PRA/PRB ratio expressed in tumor cells rendered them sensitive to MFP treatment. Thus, MFP is being tested as a novel therapy for patients with breast cancer with high expression of PRA (MIPRA; NCT02651844). Our results suggest that, in addition to endocrine-related mechanisms, antiprogestins may improve the response rate of immunotherapy in HR$^+$ breast cancer by favoring the development of a T-cell memory program. A phase II clinical trial that combines the anti–PD-1 antibody pembrolizumab together with MFP is ongoing with advanced TNBC and HR$^+$HER2^{neg} breast tumors (NCT03225547). In this trial, high doses of MFP (300 mg/day) are used to achieve antiglucocorticoid effects and potentiate the immune system (37). The novelty of our study lies in the proposal that low doses of MFP would directly evoke tissue remodeling and an ICD in PRA-H tumors that ultimately favors the immune response.

Regulation of immune responses by hormones has been widely documented in the context of fetomaternal tolerance and during autoimmunity, where progesterone ameliorates disease manifestations (38, 39). Expression of nuclear PR on T cells has been discarded in most reports, and evidence indicates that progesterone action on T cells is mediated by promiscuous binding to the glucocorticoid receptor (GR; ref. 40) or through non-genomic activation of

Published OnlineFirst December 2, 2020; DOI: 10.1158/0008-5472.CAN-20-1441

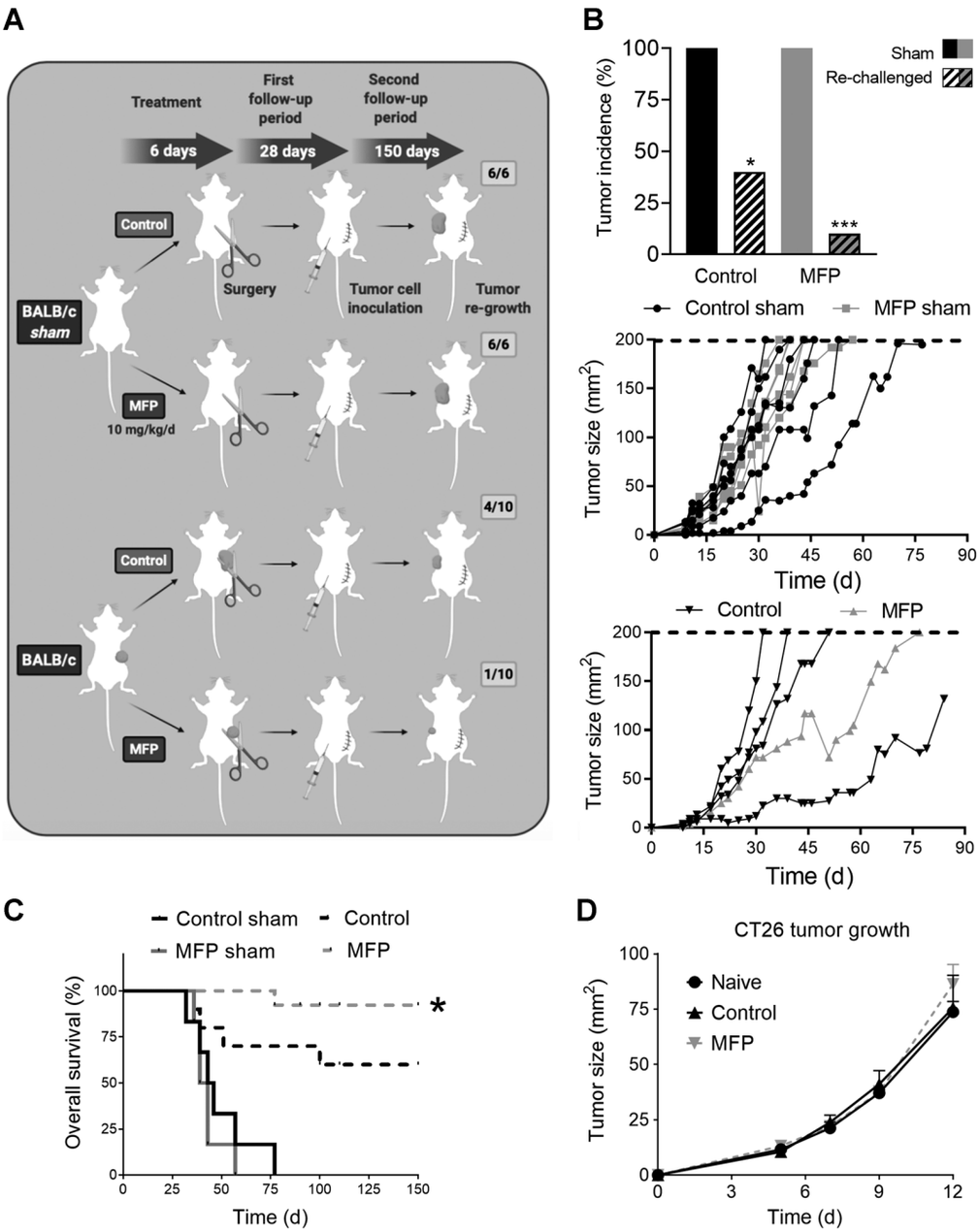

Figure 6.

MFP treatment induces an immune-protective memory in BALB/c mice. **A,** Schematic diagram of the experimental design. 59–2-HI cells were injected into the flank of BALB/c mice and were treated as depicted in **Fig. 5A**, adding a group of sham mice. Created with BioRender.com **B,** Tumor incidence indicates the percentage of animals in which a tumor was detected. Curves represent individual tumor growth kinetics. **C,** Animals were euthanized when tumors reached 200 mm^2. Overall survival of re-challenged mice is depicted in a Kaplan–Meier curve. **D,** Mice in which the secondary tumors did not grow were additionally challenged with 3×10^5 CT26 syngeneic tumor cells and tumor growth was monitored. Naïve animals were used as controls ($n = 6$–10/group). *, $P < 0.05$ between control and control sham; ***, $P < 0.001$ between MFP and MFP sham.

membrane PR (41). Notably, MFP used at high doses binds both nuclear PR and GR, thus, we can speculate that MFP may trigger immune response indirectly by inducing ICD on tumor cells by binding to the nuclear PR, or directly by inhibiting GR expressed on immune cells. However, given that we used low MFP concentrations, and the observed effect was specific for tumors expressing higher levels of PRA than PRB or High levels of PRA, the antiglucocorticoid effect seems unlikely.

The results showed herein might be extrapolated to other hormone therapies such as tamoxifen or aromatase inhibitors in the case of breast cancer or antiandrogens for prostate cancer. The role of ER on tumor immunity is controversial, whereas early studies

Published OnlineFirst December 2, 2020; DOI: 10.1158/0008-5472.CAN-20-1441

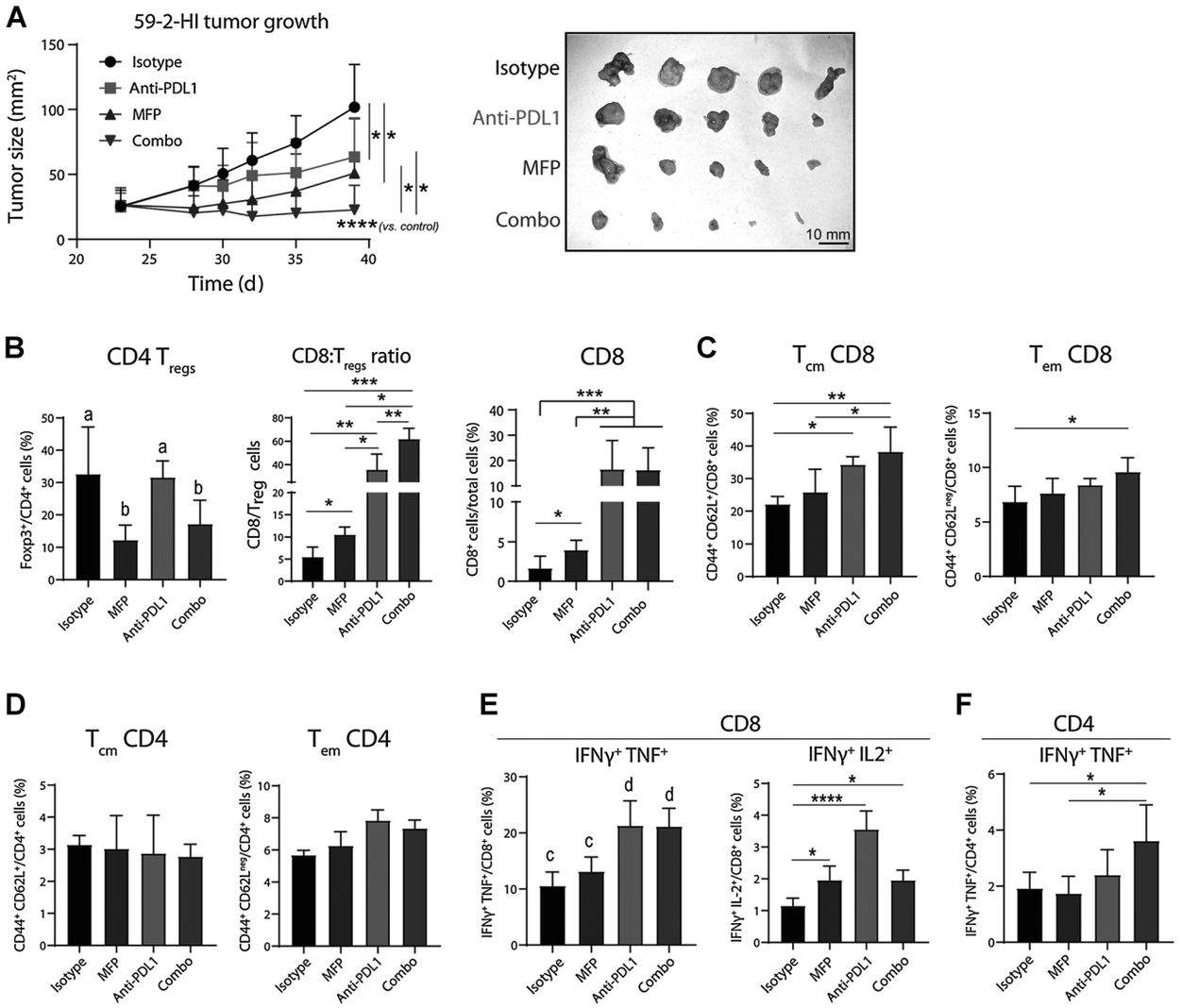

Figure 7.

MFP increases response to anti–PD-L1 treatment in HR$^+$ tumors. **A,** 59–2-HI cells were injected into the flank of immunocompetent BALB/c mice. When tumors reached 20–30 mm^2, animals were treated with low MFP doses (0.1 mg/pellet) or remained untreated. Four days later, two of the experimental groups received PD-L1 blocking antibody every two days. Tumor growth was monitored for the next two weeks (n = 5/group; left). Images of the excised tumors at the end of the experiment (right). **B,** Tumors were minced and CD8$^+$ and CD4$^+$ Foxp3$^+$ Tregs frequencies were assessed by FACS. Tregs (left) and CD8$^+$ (right) T-cell frequencies and CD8/Tregs ratio (middle) are shown. **C** and **D,** PBMCs were isolated and central- and effector-memory CD8 (**C**) and CD4 (**D**) T-cell population frequency was determined by FACS. **E** and **F,** Cytokine production after *in vitro* stimulation of PBMCs with PMA/Ionomycin was determined by FACS. The mean ± SD of a representative experiment of two is shown. *, $P < 0.05$; **, $P < 0.01$; ***, $P < 0.001$; ****, $P < 0.0001$; **a** vs. **b**, $P < 0.05$; **c** vs. **d**, $P < 0.001$.

have shown impaired proliferative capacity of CD4 T cells and NK cell cytotoxicity in tamoxifen-treated patients with breast cancer (reviewed in ref. 42), recent discoveries from Conejo-Garcia's laboratory suggest that tamoxifen could promote antitumor immunity. They found that activation of the ER promoted the expansion of MDSCs and immune escape in ovarian and breast cancer models (43). Upon tamoxifen treatment, the authors observed an enhanced antitumor immune response and tumor growth inhibition. Consequently, in the multi-arm MORPHEOUS Trial, patients with metastatic HR$^+$ breast cancer are being treated with atezolizumab combined with fulvestrant or tamoxifen (NCT03280563). Collectively, the evidence suggests that current endocrine therapies may elicit an antitumor immune response that could protect patients from relapse, contributing to the success of these therapies even after they have been interrupted. Moreover, MFP may modulate the activity of PR, GR, and androgen receptors simultaneously and this particular property that could be named "the power of three," significantly expands the application of MFP as an endocrine therapy to boost the immune response in several tumor types.

Immunotherapy has yet to achieve its full potential in breast cancer (44). Thus, to understand the immune composition of the breast TME or to identify specific immune cell populations that could improve response rates is mandatory. Positive infiltration of CD8 T cells has been associated with clinical benefit of anti–PD-1 treatment in melanoma and NSCLC, as PD-1 blockade releases the breaks on already primed cytotoxic CD8 T cells (45). The frequency of TILs in

Published OnlineFirst December 2, 2020; DOI: 10.1158/0008-5472.CAN-20-1441

TME is associated with the TMB and abundance of neoantigens (46). Nevertheless, among all breast cancer subtypes, only TNBC and $HER2^+$ tumors show a significant TMB and, consequently, a higher number of TILs (10, 47). Hence, current efforts are aimed at boosting tumor-specific immune responses that could turn immune desert HR^+ tumor into immune active tumors. Standard radiotherapies, chemotherapeutic drugs, and targeted therapies have been shown to promote antigen release, thus priming an effective adaptive immune response (48).

Our results demonstrate an underappreciated role of antiprogestins in fostering a memory T-cell response that protects from secondary outgrowths. Mechanistically, we show that MFP treatment activates in PRA-H luminal tumors an ICD program, leading to the exposure of DAMPs, specifically calreticulin and HMGB-1, which in turn activate DC maturation, leading to more efficient antigen presentation. MFP treatment significantly favored lymphocyte infiltration into the tumor bed, increasing the transcriptional activity of genes involved in pro-inflammatory pathways and reducing immunosuppressive populations as Tregs and MDSCs. These observations may reveal an essential but overlooked mechanism by which MFP indirectly elicits an immune response by regulating several immune functions, including DC activation, modulation of NK cell cytotoxicity enhancing a cellular immune response.

Within the TME, immunological exhaustion can render TILs ineffective to eliminate tumor cells (49). This might be the case of MFP-treated tumors that can also be susceptible to inhibitory checkpoints expressed by both tumor and non-tumor cells. In fact, we detected an increase in PD-1 expression among CD4 T cells in MFP-treated animals, and PD-L1 expression was induced in $CD45^{neg}$ cells and $F4/80^+$ macrophages *in vivo* upon endocrine treatment. Therefore, our results encourage the rational combination of antiprogestin therapy and ICB (particularly anti–PD-L1–targeted therapies) to prevent tumor recurrence in a subgroup of HR^+ breast cancers or in PRA-H breast cancers.

Authors' Disclosures

M. Salatino reports grants from ANPCYT and Sales Foundation during the conduct of the study. C. Lanari reports grants and non-financial support from ANPCYT and INC during the conduct of the study, as well as a patent for methods and compositions for treating antiprogestin-resistant cancers issued. No disclosures were reported by the other authors.

Authors' Contributions

G.R. Sequeira: Conceptualization, data curation, formal analysis, validation, investigation, methodology, writing-original draft. **A. Sahores:** Conceptualization, data curation, formal analysis, validation, investigation, methodology, writing-original draft. **T. Dalotto-Moreno:** Conceptualization, data curation, formal analysis, validation, investigation, methodology, writing-original draft. **R.M. Perrotta:** Data curation, software, methodology. **G. Pataccini:** Data curation, methodology. **S.I. Vanzulli:** Formal analysis, methodology. **M.L. Polo:** Data curation. **D.C. Radisky:** Data curation, methodology. **C.A. Sartorius:** Resources. **V. Novaro:** Formal analysis, supervision, writing-review and editing. **C.A. Lamb:** Formal analysis, investigation, writing-review and editing. **G.A. Rabinovich:** Conceptualization, funding acquisition, writing-review and editing. **M. Salatino:** Conceptualization, formal analysis, supervision, funding acquisition, investigation, writing-original draft, writing-review and editing. **C. Lanari:** Conceptualization, formal analysis, supervision, funding acquisition, investigation, writing-original draft, writing-review and editing.

Acknowledgments

We thank Gador, Williams, René Barón, Sales (all from Argentina), and Lounsbery Foundations for their continuous support. This study was supported by ANPCYT; grants PICT 2015–1022 and PICT 2017–2073, Ministerio de Salud, INC (2015 and 2018; to C. Lanari); PICT 2014–3687, 2017–0494 and Lounsbery Foundation (to G.A. Rabinovich). PICT 2014–0291 and 2018–02602 (to M. Salatino) and Fundación Sales (to G.A. Rabinovich and C. Lanari). Fulbright Visiting Fellowship Program 2012 (to M.L. Polo) and PICT 2015–2315 (to V. Novaro).

The costs of publication of this article were defrayed in part by the payment of page charges. This article must therefore be hereby marked *advertisement* in accordance with 18 U.S.C. Section 1734 solely to indicate this fact.

Received April 29, 2020; revised September 28, 2020; accepted November 25, 2020; published first December 2, 2020.

References

1. Chen DS, Mellman I. Oncology meets immunology: the cancer-immunity cycle. Immunity 2013;39:1–10.
2. Ribas A, Wolchok JD. Cancer immunotherapy using checkpoint blockade. Science 2018;359:1350–5.
3. Motzer RJ, Escudier B, McDermott DF, George S, Hammers HJ, Srinivas S, et al. Nivolumab versus everolimus in advanced renal-cell carcinoma. N Engl J Med 2015;373:1803–13.
4. Wolchok JD, Chiarion-Sileni V, Gonzalez R, Rutkowski P, Grob JJ, Cowey CL, et al. Overall survival with combined nivolumab and ipilimumab in advanced melanoma. N Engl J Med 2017;377:1345–56.
5. Reck M, Rodriguez-Abreu D, Robinson AG, Hui R, Csoszi T, Fulop A, et al. Pembrolizumab versus chemotherapy for PD-L1–positive non–small cell lung cancer. N Engl J Med 2016;375:1823–33.
6. Ferris RL, Blumenschein G Jr, Fayette J, Guigay J, Colevas AD, Licitra L, et al. Nivolumab for recurrent squamous-cell carcinoma of the head and neck. N Engl J Med 2016;375:1856–67.
7. Ansell SM, Lesokhin AM, Borrello I, Halwani A, Scott EC, Gutierrez M, et al. PD-1 blockade with nivolumab in relapsed or refractory Hodgkin's lymphoma. N Engl J Med 2015;372:311–9.
8. Adams S, Gatti-Mays ME, Kalinsky K, Korde LA, Sharon E, Amiri-Kordestani L, et al. Current landscape of immunotherapy in breast cancer: a review. JAMA Oncol 2019;5:1205–1214.
9. Luen S, Virassamy B, Savas P, Salgado R, Loi S. The genomic landscape of breast cancer and its interaction with host immunity. Breast 2016;29:241–50.
10. Stanton SE, Adams S, Disis ML. Variation in the incidence and magnitude of tumor-infiltrating lymphocytes in breast cancer subtypes: a systematic review. JAMA Oncol 2016;2:1354–60.
11. Loi S, Sirtaine N, Piette F, Salgado R, Viale G, Van Eenoo F, et al. Prognostic and predictive value of tumor-infiltrating lymphocytes in a phase III randomized adjuvant breast cancer trial in node-positive breast cancer comparing the addition of docetaxel to doxorubicin with doxorubicin-based chemotherapy: BIG 02–98. J Clinical Oncol 2013;31:860–7.
12. Sharma P, Allison JP. Immune checkpoint targeting in cancer therapy: toward combination strategies with curative potential. Cell 2015;161:205–14.
13. Krysko DV, Garg AD, Kaczmarek A, Krysko O, Agostinis P, Vandenabeele P. Immunogenic cell death and DAMPs in cancer therapy. Nat Rev Cancer 2012;12:860–75.
14. McGuire WL. Hormone receptors: their role in predicting prognosis and response to endocrine therapy. Semin Oncol 1978;5:428–33.
15. Rojas PA, May M, Sequeira GR, Elia A, Alvarez M, Martinez P, et al. Progesterone receptor isoform ratio: a breast cancer prognostic and predictive factor for antiprogestin responsiveness. J Natl Cancer Inst 2017;109:djw317.
16. Lamb CA, Fabris VT, Jacobsen B, Molinolo AA, Lanari C. Biological and clinical impact of imbalanced progesterone receptor isoform ratios in breast cancer. Endocr Relat Cancer 2018;10:ERC–18–0179.
17. Sartorius CA, Groshong SD, Miller LA, Powell RL, Tung L, Takimoto GS, et al. New T47D breast cancer cell lines for the independent study of progesterone B- and A-receptors: only antiprogestin-occupied B-receptors

are switched to transcriptional agonists by cAMP. Cancer Res 1994;54: 3868–77.
18. Lanari C, Lamb CA, Fabris VT, Helguero LA, Soldati R, Bottino MC, et al. The MPA mouse breast cancer model: evidence for a role of progesterone receptors in breast cancer. Endocr Relat Cancer 2009;16:333–50.
19. Fabris VT, Sahores A, Vanzulli SI, Colombo L, Molinolo AA, Lanari C, et al. Inoculated mammary carcinoma-associated fibroblasts: contribution to hormone independent tumor growth. BMC Cancer 2010;10:293.
20. Sartorius CA, Shen T, Horwitz KB. Progesterone receptors A and B differentially affect the growth of estrogen-dependent human breast tumor xenografts. Breast Cancer Res and Treat 2003;79:287–99.
21. Sequeira G, Vanzulli SI, Rojas P, Lamb C, Colombo L, May M, et al. The effectiveness of nano chemotherapeutic particles combined with mifepristone depends on the PR isoform ratio in preclinical models of breast cancer. Oncotarget 2014;5:3246–60.
22. Dalotto-Moreno T, Croci DO, Cerliani JP, Martinez-Allo VC, Dergan-Dylon S, Mendez-Huergo SP, et al. Targeting galectin-1 overcomes breast cancer-associated immunosuppression and prevents metastatic disease. Cancer Res 2013;73:1107–17.
23. Wargon V, Riggio M, Giulianelli S, Sequeira GR, Rojas P, May M, et al. Progestin and antiprogestin responsiveness in breast cancer is driven by the PRA/PRB ratio via AIB1 or SMRT recruitment to the CCND1 and MYC promoters. Int J Cancer 2015;136:2680–92.
24. Ilarregui JM, Croci DO, Bianco GA, Toscano MA, Salatino M, Vermeulen ME, et al. Tolerogenic signals delivered by dendritic cells to T cells through a galectin-1–driven immunoregulatory circuit involving interleukin 27 and interleukin 10. Nat Immunol 2009;10:981–91.
25. Polo ML, Riggio M, May M, Rodriguez MJ, Perrone MC, Stallings-Mann M, et al. Activation of PI3K/Akt/mTOR signaling in the tumor stroma drives endocrine therapy-dependent breast tumor regression. Oncotarget 2015;6: 22081–97.
26. Garg AD, De Ruysscher D, Agostinis P. Immunological metagene signatures derived from immunogenic cancer cell death associate with improved survival of patients with lung, breast or ovarian malignancies: a large scale meta-analysis. Oncoimmunology 2016;5:e1069938.
27. Bezu L, Gomes-de-Silva LC, Dewitte H, Breckpot K, Fucikova J, Spisek R, et al. Combinatorial strategies for the induction of immunogenic cell death. Front Immunol 2015;6:187.
28. DeSantis CE, Ma J, Gaudet MM, Newman LA, Miller KD, Goding Sauer A, et al. Breast cancer statistics, 2019. CA Cancer J Clin 2019;69:438–51.
29. Schmid P, Adams S, Rugo HS, Schneeweiss A, Barrios CH, Iwata H, et al. Atezolizumab and nab-paclitaxel in advanced triple-negative breast cancer. N Engl J Med 2018;379:2108–21.
30. Waks AG, Stover DG, Guerriero JL, Dillon D, Barry WT, Gjini E, et al. The immune microenvironment in hormone receptor-positive breast cancer before and after preoperative chemotherapy. Clin Cancer Res 2019;25:4644–55.
31. Ito M, Hiramatsu H, Kobayashi K, Suzue K, Kawahata M, Hioki K, et al. NOD/SCID/gamma(c)(null) mouse: an excellent recipient mouse model for engraftment of human cells. Blood 2002;100:3175–82.
32. Ishikawa F, Yasukawa M, Lyons B, Yoshida S, Miyamoto T, Yoshimoto G, et al. Development of functional human blood and immune systems in NOD/SCID/IL2 receptor {gamma} chain(null) mice. Blood 2005;106:1565–73.
33. Kidd S, Spaeth E, Watson K, Burks J, Lu H, Klopp A, et al. Origins of the tumor microenvironment: quantitative assessment of adipose-derived and bone marrow-derived stroma. PLoS ONE 2012;7:e30563.
34. Worthley DL, Si Y, Quante M, Churchill M, Mukherjee S, Wang TC. Bone marrow cells as precursors of the tumor stroma. Exp Cell Res 2013;319:1650–6.
35. Verbiest T. FR, Brown N, Finnon P, Bouffler S, Badie C. NOD scid gamma mice are permissive to allogeneic HSC transplantation without prior conditioning. Int J Mol Sci 2016;17:1850.
36. Gonzalez-Suarez E, Jacob AP, Jones J, Miller R, Roudier-Meyer MP, Erwert R, et al. RANK ligand mediates progestin-induced mammary epithelial proliferation and carcinogenesis. Nature 2010;468:103–7.
37. Fleseriu M, Biller BM, Findling JW, Molitch ME, Schteingart DE, Gross C. Mifepristone, a glucocorticoid receptor antagonist, produces clinical and metabolic benefits in patients with Cushing's syndrome. J Clin Endocrinol Metab 2012;97:2039–49.
38. Spallanzani RG, Dalotto-Moreno T, Raffo IX, Ziblat A, Domaica CI, Avila DE, et al. Expansion of CD11b(+)Ly6G (+)Ly6C (int) cells driven by medroxyprogesterone acetate in mice bearing breast tumors restrains NK cell effector functions. Cancer Immunol Immunother 2013;62:1781–95.
39. Blois SM, Ilarregui JM, Tometten M, Garcia M, Orsal AS, Cordo-Russo R, et al. A pivotal role for galectin-1 in fetomaternal tolerance. Nat Med 2007;13: 1450–7.
40. Engler JB, Kursawe N, Solano ME, Patas K, Wehrmann S, Heckmann N, et al. Glucocorticoid receptor in T cells mediates protection from autoimmunity in pregnancy. Proc Natl Acad Sci U S A 2017;114:E181–E90.
41. Tan IJ, Peeva E, Zandman-Goddard G. Hormonal modulation of the immune system—a spotlight on the role of progestogens. Autoimmun Rev 2015;14: 536–42.
42. Behjati S, Frank MH. The effects of tamoxifen on immunity. Curr Med Chem 2009;16:3076–80.
43. Svoronos N, Perales-Puchalt A, Allegrezza MJ, Rutkowski MR, Payne KK, Tesone AJ, et al. Tumor cell-independent estrogen signaling drives disease progression through mobilization of myeloid-derived suppressor cells. Cancer Discov 2017;7:72–85.
44. Planes-Laine G, Rochigneux P, Bertucci F, Chretien AS, Viens P, Sabatier R, et al. PD-1/PD-L1 targeting in breast cancer: the first clinical evidences are emerging. A Literature Review. Cancers 2019;11:1033.
45. Uryvaev A PM, Hershkovits D, Sabo E, Bar-Sela G. The role of tumor-infiltrating lymphocytes (TILs) as a predicitive biomarker of response to anti-PD1 therapy in patients with metastatic non–small cell lung cancer or metastatic melanoma. Med Oncol 2018;35:25.
46. McGranahan N, Furness AJ, Rosenthal R, Ramskov S, Lyngaa R, Saini SK, et al. Clonal neoantigens elicit T-cell immunoreactivity and sensitivity to immune checkpoint blockade. Science 2016;351:1463–9.
47. Alexandrov LB, Nik-Zainal S, Wedge DC, Aparicio SA, Behjati S, Biankin AV, et al. Signatures of mutational processes in human cancer. Nature 2013; 500:415–21.
48. Garg AD, More S, Rufo N, Mece O, Sassano ML, Agostinis P, et al. Trial watch: Immunogenic cell death induction by anticancer chemotherapeutics. Oncoimmunology 2017;6:e1386829.
49. Jiang Y, Li Y, Zhu B. T-cell exhaustion in the tumor microenvironment. Cell Death Dis 2015;6:e1792.

Published OnlineFirst December 2, 2020; DOI: 10.1158/0008-5472.CAN-20-1441

Cancer Research
The Journal of Cancer Research (1916–1930) | The American Journal of Cancer (1931–1940)

AACR American Association for Cancer Research

Enhanced Antitumor Immunity via Endocrine Therapy Prevents Mammary Tumor Relapse and Increases Immune Checkpoint Blockade Sensitivity

Gonzalo R. Sequeira, Ana Sahores, Tomás Dalotto-Moreno, et al.

Cancer Res 2021;81:1375-1387. Published OnlineFirst December 2, 2020.